On relative distortion in fingerprint comparison

Nathan D. Kalka *, R. Austin Hicklin

Noblis, 3150 Fairview Park Drive, Falls Church, VA 22043, USA

ARTICLE INFO

ABSTRACT

When fingerprints are deposited, non-uniform pressure in conjunction with the inherent elasticity of friction ridge skin often causes linear and non-linear distortions in the ridge and valley structure. The effects of these distortions must be considered during analysis of fingerprint images. Even when individual prints are not notably distorted, relative distortion between two prints can have a serious impact on comparison. In this paper we discuss several metrics for quantifying and visualizing linear and non-linear fingerprint deformations, and software tools to assist examiners in accounting for distortion in fingerprint comparisons.

© 2014 Elsevier Ireland Ltd. All rights reserved.

1. Introduction

When fingerprints[1] [1–6] are deposited, variations in pressure in conjunction with the inherent elasticity of friction ridge skin often cause linear and non-linear distortions in the resulting ridge and valley structure. When a three-dimensional finger is applied to a two-dimensional surface, the resulting image is generally distorted with respect to the original skin. Distortions in the fingerprint can be caused by the substrate (e.g. curved or flexible objects), matrix (e.g. viscous substances), development medium (e.g. powder buildup), and the pressure and direction of deposition [7]. Deposition pressure (downward pressure) can change the width of ridges and valleys, as well as the appearance of minutiae, ridge edge details, and pores [8]. Shearing (lateral pressure in a single direction) will cause elongation or compression of the print, resulting in linear differences in the location of minutiae or other features. The most complex non-linear distortions are caused by torque (twisting pressure), which can cause apparent changes in the overall pattern as well as substantial differences in the relative locations of features [9]. Latent fingerprints can be highly distorted due to the combination of some or all of these factors. Exemplars also can be distorted, particularly in the upper corners of rolled prints.

Anatomical constraints affect how the finger pad reacts to pressure. Areas in the center of the finger can distort more than the less flexible tips or edges. The ability of skin to stretch or compress is affected by the direction of ridge flow: skin is less flexible in the direction of ridge flow than perpendicular to flow. Therefore cores and deltas respond differently to pressure than open fields of parallel ridges, and different pattern types react differently to pressure [9]. The effects of pressure and finger deformation may or may not be apparent in the analysis of a single impression. However, even when individual prints do not appear to be distorted, the relative distortion between two prints can have a serious impact on comparison.

Here we model the linear and non-linear relative distortion between pairs of latent and exemplar prints. The models are based on the annotation of corresponding minutiae by latent print examiners, to provide tools to assist in fingerprint comparison. These models are used in the implementation of "ghost cursor" functionality in the Federal Bureau of Investigation's (FBI's) Universal Latent Workstation (ULW) [10]: for any cursor location in one image, the ghost cursor is shown at the estimated corresponding location in the other image. We also show how the models can be used in visualization tools, and in metrics quantifying the extent of distortion.

---

* Corresponding author. Tel.: +1 304 848 3918.
E-mail addresses: nathan.kalka@noblis.org (N.D. Kalka),
hicklin@noblis.org (R.A. Hicklin).
[1] Regarding the use of terminology – "latent print" is the preferred term in North America for a friction ridge impression from an unknown source, and "print" is used to refer generically to known or unknown impressions [1]. We recognize that outside of North America, the preferred term for an impression from an unknown source is "mark" or "trace," and that "print" is used to refer only to known impressions. We are using the North American standard terminology to maintain consistency with our previous and future papers in this series [2–6].

2. Background

The presence of elastic distortion in fingerprints plays a significant role in automated fingerprint matching algorithms. These algorithms automatically determine the similarity or correspondence between friction ridge impressions [11,12]. In most cases, the pairwise similarity is computed by analyzing the spatial distribution of minutia points. If the minutiae from two impressions are very similar then the algorithm returns a relatively high score, implying a high probability that they are from the same source. Early fingerprint matching algorithms would determine the similarity between minutia sets based on an affine registration model. Affine models can be decomposed into rigid, semi-rigid, or full-affine. Rigid models account for translation and rotation. Semi-rigid models include the addition of uniform scaling. In the literature, semi-rigid models are often referred to as similarity transforms. Full affine models additionally account for non-uniform scaling and skew. Thus, non-linear distortions resulting from the elastic nature of friction ridge skin were unaccounted for, often resulting in poor or suboptimal correspondence between the minutia sets. Great strides have been made with respect to mitigating non-linear distortion in automated fingerprint recognition systems. These approaches can be generalized into two categories. Implicit strategies typically mitigate distortion during the matching stage by relaxing constraints with respect to the geometric relationships between minutiae sets. On the other hand, explicit strategies estimate distortion prior to matching, thereby allowing minutiae to be pre-distorted, typically via a non-linear transform.

In [12], an adaptive elastic matching algorithm was proposed that utilizes tolerance boxes and string matching. The authors note that non-linear deformation present in fingerprints has a tendency to radiate outward from the center of deformed print regions. Thus, the tolerance boxes are iteratively increased moving outward from the center of deformed regions. Watson and Casasent [13] explored several correlation filters designed specifically to provide robustness against fingerprint distortion. Each filter is generated from training on several impressions of the same finger. Thus, variability across the different impressions can be captured within the filter. The authors report that their filter approach compares favorably to traditional minutiae matching based approaches.

Non-linear warping techniques have been explored to explicitly account for the relative distortion between a pair of impressions. That is, warping provides the ability for distortion to be estimated and removed prior to final stage minutiae matching. Note that warping strategies require corresponding minutia sets that are determined by automated feature extraction algorithms or by humans. Therefore, the accuracy of the models used for warping depends on the precision and correctness of the corresponding minutia. Another limitation with warping strategies is that they are susceptible to excessive deformation if unrelated minutiae are treated as if they are corresponding: metrics such as bending energy are used to detect such excessive deformation. In [14,15], the Thin Plate Spline (TPS) [16] warping algorithm was applied to mitigate fingerprint distortion. In particular, TPS was applied to non-rigidly align the minutiae sets to increase matching performance. Given several impressions of the same finger, Ross et al. [17,18] utilized the TPS algorithm for creating an average deformation model based on minutiae and ridge curve correspondences. The estimated average deformation is then used to pre-distort minutiae prior to a final matching stage. Novikov and Ushmaev [19] propose the numerical solution of the Navier linear PDE as an alternative to TPS. They argue that their approach is more robust than TPS when only a small number of corresponding minutiae are available. Similarly, Liang et al. [20] apply a multi-quadratic radial basis function instead of the traditional TPS basis function. The multi-quadratic function provides better local support. That is, the magnitude of the warp is much weaker in regions where minutiae are sparse. In contrast, the magnitude of the warp is much greater in regions where the spatial distribution of minutiae is dense.

Warping strategies require a correspondence between minutiae sets in order to estimate deformation and subsequently mitigate the extent of distortion. An alternative to warping, that does not require minutiae point correspondence, is impression normalization. More specifically, distortion is corrected a priori, such that traditional matching algorithms can be used. In [21], Senior and Bolle provided an approach that normalizes the ridge skeleton of an impression such that the distance between all ridges is equally spaced. This approach handles compressive or expansive distortions orthogonal to the direction of the ridge flow fairly well. However, distortions of the ridge flow along the primary ridge direction are not mitigated.

3. Approach

In this paper, we develop metrics and visualization tools that can be used to assist examiners with linear and non-linear distortions during latent fingerprint comparison. To achieve this, we adopted a strategy from the category of explicit approaches, notably, warping. Our warping strategy utilizes manually annotated minutia correspondences between a latent and exemplar print. As with all warping strategies, we first globally align the correspondences through an affine transform. Following this, the TPS algorithm is applied to quantify the relative non-linear deformation between the minutia correspondences.

We then aggregate metrics and image representations from the linear and TPS models for visualizing relative distortion. The following subsections detail this approach.

3.1. Global pre-alignment

Prior to estimating the relative non-rigid deformation, we establish a global alignment between the corresponding minutiae sets in the latent and exemplar print via an affine transformation as in Mital et al. [22].

Let $E = (e_1, e_2, \ldots, e_N)^T$ and $L = (l_1, l_2, \ldots, l_N)^T$ represent the corresponding minutiae point pairs from the exemplar and latent print, respectively. The coordinates of latent points, L, can be expressed in terms of the coordinates of exemplar points, E, as follows:

$$E = AL + t,$$

where A is a 2×2 linear matrix and a 2×1 vector t. A planar affine transformation is described by 6 parameters which account for rotation, scale, shear, and translation. Thus, the transformation can be determined from 3 pairs of corresponding minutiae points by solving for the coefficients of matrix A and the translation vector t:

$$E_x = a_{11}L_x + a_{12}L_y + t_1$$
$$E_y = a_{21}L_x + a_{22}L_y + t_2.$$

We opted for a least squares approach for estimating both A and t, based on examiners' marking of three or more corresponding points. Thus, matrix A is then estimated as follows:

$$A = \tilde{E}\tilde{L}^T(\tilde{L}\tilde{L}^T)^{-1},$$

where $\tilde{E}$ and $\tilde{L}$ represent the exemplar and latent points after mean centering, and T corresponds to a matrix transpose operator. The translation vector, t, is calculated as:

$$t = \bar{E} - A\bar{L},$$

by computing the centroid of each point set, $\bar{E}$ and, $\bar{L}$ and taking the difference.

3.2. Thin plate splines

Having determined the affine alignment based on the minutia correspondences, we next construct a thin plate spline (TPS) model to estimate the relative non-linear deformation, f, between the correspondences. The warping function f interpolates the point correspondences (l_i, e_i), that is, $f(l_i) = e_i, \forall i = 1, 2, \ldots, N$.

$$f(l) = Al + W^T s(l),$$

where A is a 3×2 affine matrix, W^T is a $N \times 2$ coefficient matrix, and $s(l) = [U(l - l_1), U(l - l_2), \ldots, U(l - l_N)]^T$ where $U(l) = l^2 \log(l^2)$. The warping function f minimizes the TPS deformation energy $R(f)$:

$$R(f) = \iint \left(\left(\frac{\partial^2 f}{\partial x^2} \right)^2 + 2 \left(\frac{\partial^2 f}{\partial x \, \partial y} \right)^2 + \left(\frac{\partial^2 f}{\partial y^2} \right)^2 \right) dx \, dy,$$

which ensures that each point in the latent impression is mapped to its corresponding point in the exemplar impression. The parameters of the TPS model are calculated by solving the following linear system of equations:

$$\begin{aligned} KW + P^T A &= V \\ PW &= 0 \end{aligned},$$

where K, P, V are defined as:

$$K_{ij} = \begin{cases} U(l_i - l_j), & i \neq j \\ 0 & i = j \end{cases},$$

$$P = \begin{pmatrix} 1 & l_{x1} & l_{y1} \\ 1 & l_{x2} & l_{y2} \\ \vdots & \vdots & \vdots \\ 1 & l_{xn} & l_{yn} \end{pmatrix}^T,$$

$$V = \begin{pmatrix} e_{x1} & e_{x2} & \ldots & e_{xN} \\ e_{y1} & e_{y2} & \ldots & e_{yN} \end{pmatrix}^T.$$

Here, (l_x, l_y) and (e_x, e_y) are the xy-coordinates of the minutiae in the latent and exemplar impression, respectively. For in-depth examples and a review of the TPS mathematics, the reader is referred to [16]. An example of global alignment and TPS warping is demonstrated in Fig. 1.
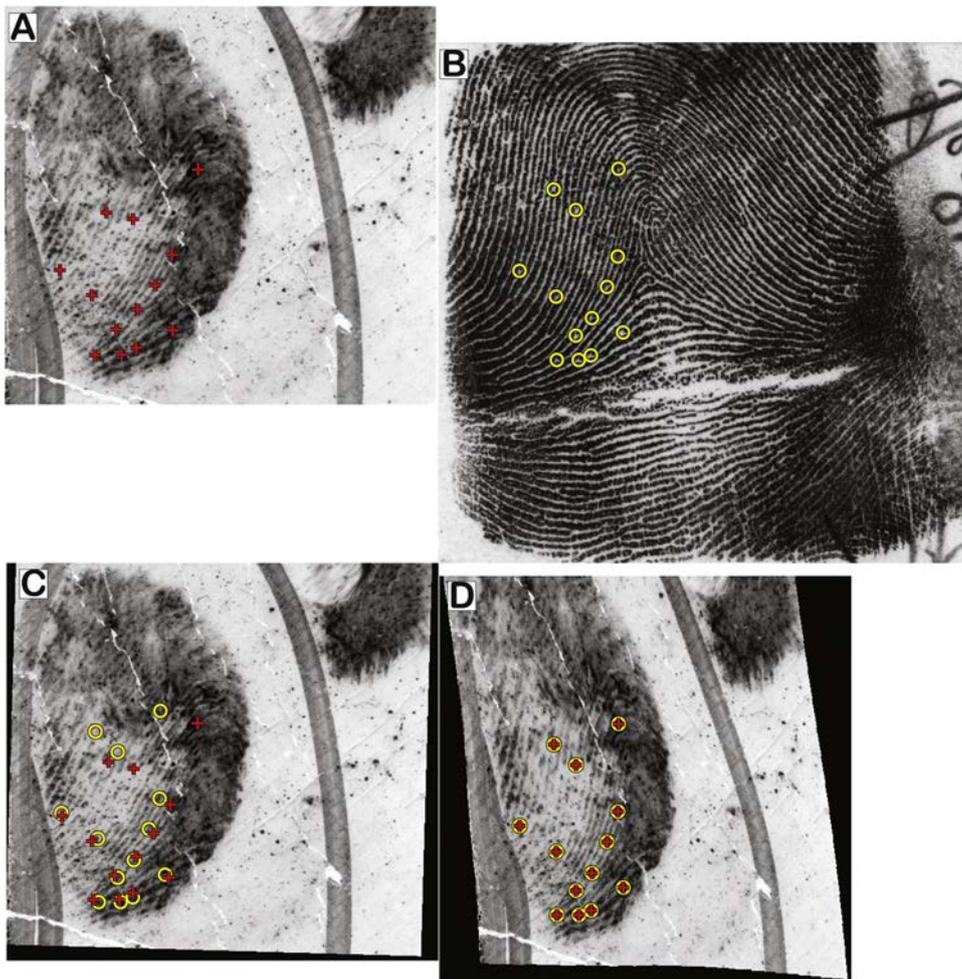
Fig. 1. (A) Latent impression overlaid with minutiae (crosses). (B) Exemplar impression overlaid with minutiae (circles). (C) Latent impression after affine registration determined from corresponding minutiae in both the latent and the exemplar. Note that alignment is poor near the cluster of minutiae in the center of the impression. (D) Registered latent impression that has been transformed with the described TPS model so that all latent minutiae (crosses) overlay precisely the exemplar minutiae (circles). (Note that images A–D are aligned vertically and horizontally with respect to the top right minutia.)

3.3. Metrics

We now describe two metrics that may be used to characterize the relative deformation between a set of impressions: (1) a Euclidean metric that captures the residual distance between corresponding minutiae points after affine registration (restricted to translation, rotation, and uniform scale), and (2) the bending energy metric which is provided through the TPS model. Residual distance accounts for both linear and non-linear distortion, whereas bending energy accounts only for non-linear distortion.

Recall that affine transformations between minutiae sets often result in poor alignment because of the way friction ridge skin deforms during deposition. Thus, the resulting residuals may be used as an indicator for deformation. The summation of these residuals can be thought of as a measure that quantifies the distance required for perfect alignment. Residual distance, *RD*, is calculated as follows:

$$RD = \frac{\sum_{i=1}^{N} \sqrt{\left(l'_{xi} - e_{xi}\right)^2 + \left(l'_{yi} - e_{yi}\right)^2}}{N},$$

where l' and e correspond to the x,y-coordinates of latent points (after semi-rigid registration) and exemplar points, respectively. The total number of corresponding points is represented here by N. Higher values of the residual distance measure indicate a stronger presence of relative deformation while lower values imply the opposite. Residual distance accounts for both linear and non-linear distortion (after accounting for rigid linear distortions).

The TPS bending energy metric is an approximate measure to the deformation energy $R(f)$. Bending energy accounts only for non-linear distortion (after accounting for affine linear distortions). This expression is equivalent to:

$$R(f) = \frac{W^T P W}{N}.$$

Fig. 2 provides an illustration of the residual distance and the bending energy metrics when applied to minutiae sets from latent and corresponding exemplar impressions in the NIST SD27 data set [23] (using the "match" corresponding minutiae). Fig. 2 also shows how erroneous corresponding points affect the metrics. We found that residual distance values above 20 were generally associated with erroneous correspondences, as were bending energy values above 0.2.

Manually annotated minutia correspondences between a latent and exemplar print are limited by human factors, and therefore could include erroneous correspondences, either through accident or errors in expertise. Distortion metrics can be used to flag potentially erroneous correspondences, as very high values of either residual distance or bending energy indicate amounts of distortion that would be improbable or impossible in correctly annotated minutia correspondences. For evaluation, we deliberately created latent-exemplar pairs with erroneous correspondences. Each set consisted of twelve latent-exemplar pairs from the NIST SD27 data set. Errors were introduced by selecting a correspondence at random, and then swapping the latent points from the nearest neighboring correspondence. For each image pair, four erroneous markups were created, with two, four, six, and eight incorrect correspondences. Multiple swaps of the same point were not allowed.

4. Visualization tools – grid warps and heat maps

The TPS modeling approach described in the previous section provides the ability to quantify relative deformation between two impressions, provided correspondences such as minutiae are marked in the impressions. Furthermore, the TPS modeling approach can be used to transform one impression so that it can be overlaid on the other, after the relative deformation is estimated as illustrated in Fig. 1. The transformed impression can be used for visualizing relative distortion but the visual cues may be difficult to observe depending on the impression background and clarity of the ridge flow. To that end, we introduce grid warps and heat maps for visualizing the relative deformation between two impressions.

The grid warp is a simple and straightforward strategy for visualizing relative deformation. Once the affine parameters and warping function f have been estimated, they are used in sequence to warp a 2D grid of vertical and horizontal lines. The warped grids provide a strong visual cue for local deformation within the impression.

The heat map is another method for visualizing relative deformation between impressions, which makes use of the residual distance metric. Instead of computing the distance
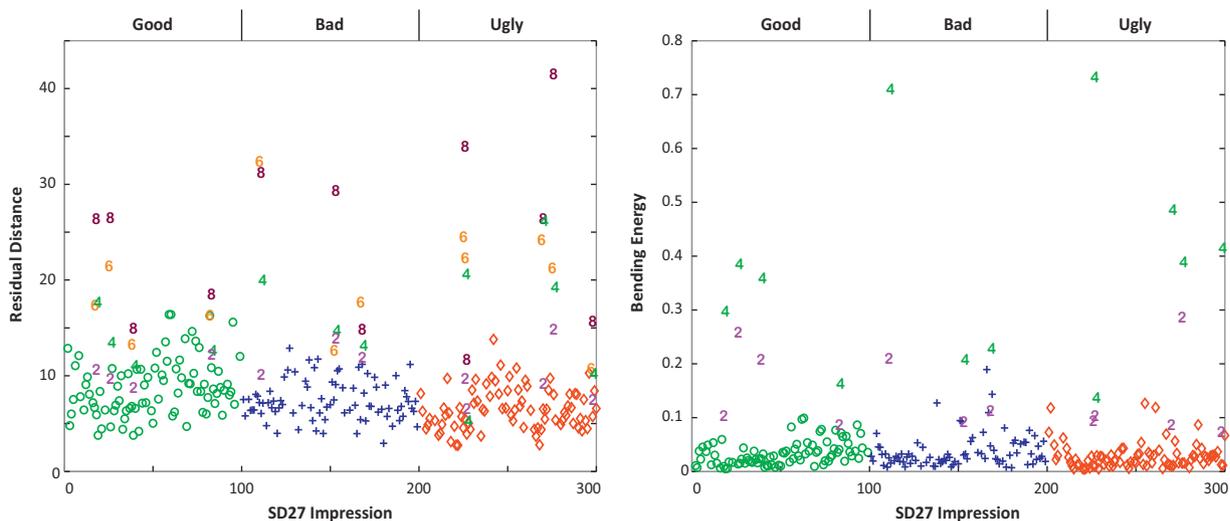
Fig. 2. Illustrates plots of the residual distance and bending energy metrics for the NIST SD27 data set [23]. Both metrics are monotonic with respect to deformation (a higher value indicates stronger deformation). The circles represent those impressions that were characterized by an examiner as "good", while the crosses and diamonds indicate "bad" and "ugly", respectively. The numbers represent impressions in which there were (deliberate) errors in corresponding minutiae, indicating 2, 4, 6, and 8 correspondence errors, respectively. Note that for bending energy, the sets with six or eight correspondence errors were in the range 0.2338–2.281, all above the maximum bending energy for the set that did not have correspondence errors, and therefore not shown.
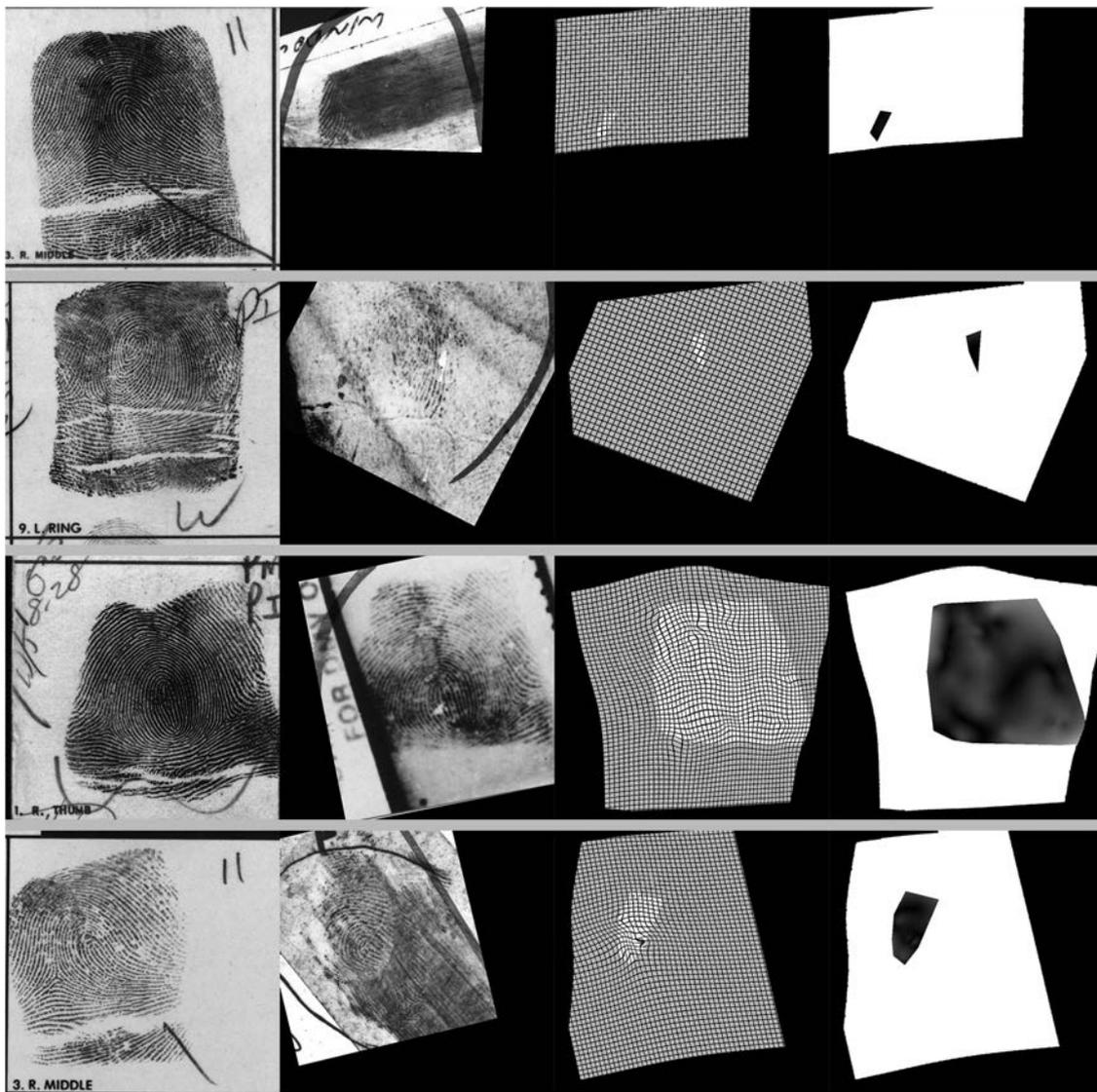
Fig. 3. Examples of grid warps and heat maps. (Column 1) exemplar; (Column 2) corresponding latent impression aligned with the exemplar through an affine transformation; (Column 3) grid warp using the TPS warping function estimated from the latent and exemplar impression, with convex hull of the warped minutiae points highlighted; (Column 4) heat map of the deformation.

between minutiae, we compute the Euclidean distance between the TPS warp and the affine transformed coordinate spaces. Thus, the magnitude of the distance is used as a visual cue for relative deformation. Note that regions in the impression that do not contain minutiae may not provide an accurate representation of the relative deformation. Therefore, once the distances have been computed, we apply a binary mask to the heat map which is restricted to the convex hull of the warped minutiae points. Higher intensity values in the map indicate higher levels of deformation while the opposite is true for lower values. Fig. 3 provides an illustration of the grid warps and heat maps. The first row corresponds to SD27 impression 222U which was characterized by residual distance metric as having the least relative deformation (*Residual distance* = 2.74; *Bending energy* = 0.0062). The second row corresponds to impression 221U, which had the least relative deformation as ranked by the bending energy metric (*Residual distance* = 2.76; *Bending energy* = 0.0046). The third row corresponds to impression 059G which was ranked by the residual distance metric as having the greatest relative deformation (*Residual distance* = 16.40; *Bending energy* = 0.0505). Lastly, the fourth row corresponds to impression 166B which was ranked by

the bending energy metric as having the greatest relative deformation (*Residual distance* = 10.89; *Bending energy* = 0.1894).

5. ULW ghost cursor

One difficulty often encountered during fingerprint comparison is that when the examiner's eyes are moving between two images, it is easy to lose track of the specific locations being compared. For non-computer comparisons (i.e. using paper fingerprint cards, photographs of latent prints, or physical evidence), examiners would use various tools to provide reference points, including pointers (such as dissecting needles), transparent disks with inscribed lines or circles (Battley disk), or paper or metal plates to block out extraneous areas. For computer comparisons, examiners can use software annotations to serve as references, but these do not serve well when performing comparisons of potentially corresponding regions before anchor points have been established; some examiners will still use physical pointers (such as two pencils) to keep track of locations in both prints.

In the ULW Comparison Tool, the warping technique described here is used in the implementation of a "ghost cursor". The user
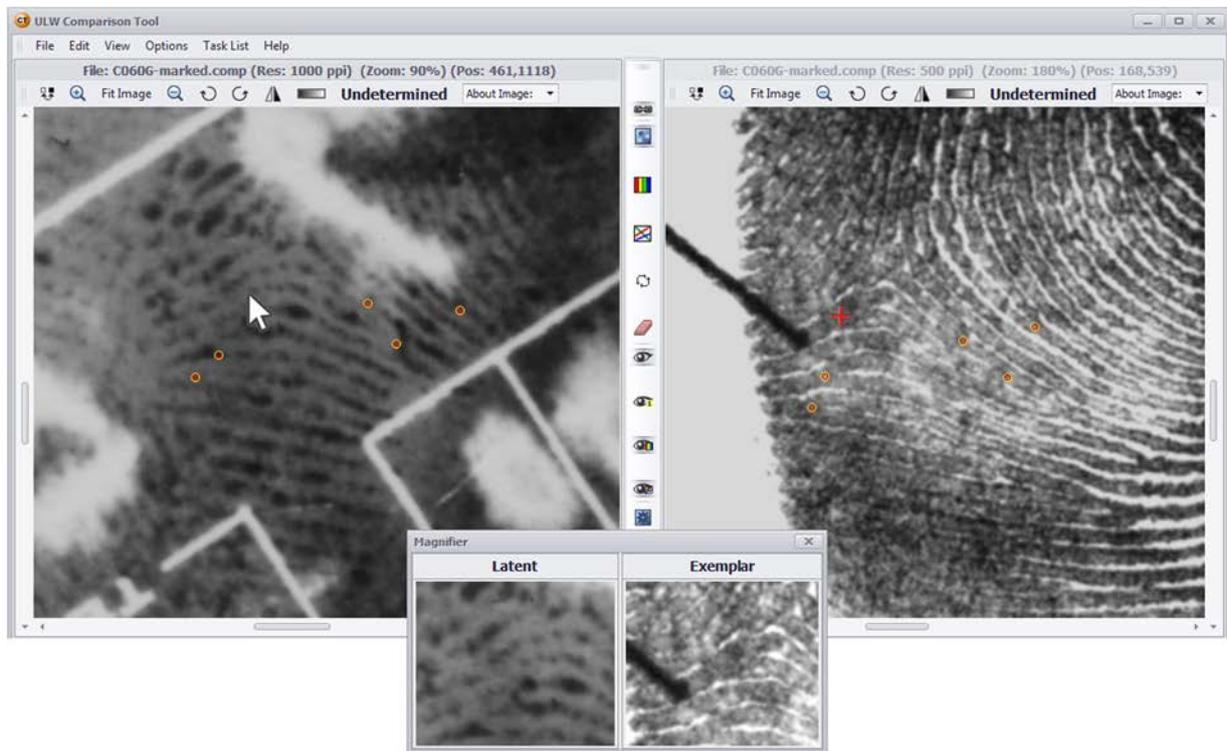
Fig. 4. Example of ghost cursor in ULW Comparison Tool. The cursor (arrow in left image) and corresponding points (circles), are used by the software to display a ghost cursor (cross in right image) at the estimated corresponding location. The magnifier is shown at the bottom.

marks corresponding features as defined in the ANSI/NIST-ITL 1-2011 standard [24], using the Comparison (COMP) transaction described in the Latent Interoperability Transmission Specification [25]. Using the corresponding points marked by the examiner, the software defines a distortion model to map projected correspondences between locations in the two images; a minimum of three points is required. Wherever the user places the cursor, the software will display a ghost cursor at the estimated corresponding location, as shown in Fig. 4. Since the ghost cursor is displayed in real time, the examiner can use it while moving the cursor to follow ridges and count ridges.

In comparing prints, the distance between the areas being compared can be problematic: it is much easier to perform a detailed comparison when the areas being compared are immediately next to each other. ULW addresses this problem with "magnifier" functionality (Fig. 4): when the user chooses to display the magnifier, the areas immediately around the cursor and ghost cursor are displayed side by side. The magnifier is not static, but tracks cursor movement about the image, allowing detailed comparison when following the sequence of ridges.

An early version of the ghost cursor was demonstrated at the 2008 International Association for Identification [26], using Delaunay triangulation for the transformation, which was much less effective than the TPS approach used here. The TPS-based ghost cursor works well in areas near corresponding points, but becomes less effective as the cursor moves farther away from corresponding features. Feedback from examiners has indicated that the ghost cursor and magnifier have been found to be useful as optional tools to assist in performing comparisons; menu and keyboard shortcuts allow them to be easily hidden when not desired.

6. Summary and discussion

In this paper we presented visualization tools and metrics that can be used to characterize the relative deformation between two

impressions, as well as software tools derived from these distortion metrics. We believe that these tools may be of benefit if used as part of an agency's quality assurance procedures. For individual examiners, the ghost cursor and magnifier software tools that are made possible by these distortion models address usability issues in performing comparisons, and also can be used as integrity checks during comparison, by identifying potentially erroneous corresponding points. For supervisors, such visualization tools and metrics can be used to flag comparisons that are especially distorted, which then could be required to have additional review or other quality assurance procedures.

References

[1] Scientific Working Group on Friction Ridge Analysis, Study and Technology; Standard terminology of friction ridge examination, ver.3.0, 2011, http://swgfast.org/documents/terminology/110323_Standard-Terminology_3.0.pdf.
[2] B.T. Ulery, R.A. Hicklin, J. Buscaglia, M.A. Roberts, Accuracy and reliability of forensic latent fingerprint decisions, Proc. Natl. Acad. Sci. U. S. A. 108 (19) (2011) 7733–7738., http://www.pnas.org/content/108/19/7733.full.pdf.
[3] R.A. Hicklin, et al., Latent fingerprint quality: a survey of examiners, J. Forensic Ident. 61 (4) (2011) 385–418.

[4] B.T. Ulery, R.A. Hicklin, J. Buscaglia, M.A. Roberts, Repeatability and reproducibility of decisions by latent fingerprint examiners, PLOS ONE 7 (3) (2012), http://www.plosone.org/article/info:doi/10.1371/journal.pone.0032800.

[5] B.T. Ulery, R.A. Hicklin, G.I. Kiebuzinski, M.A. Roberts, J. Buscaglia, Understanding the sufficiency of information for latent fingerprint value determinations, Forensic Sci. Int. 230 (1) (2013) 99–106.

[6] R.A. Hicklin, J. Buscaglia, M.A. Roberts, Assessing the clarity of friction ridge impressions, Forensic Sci. Int. 226 (1) (2013) 106–117.

[7] D. Ashbaugh, Quantitative–Qualitative Friction Ridge Analysis: An Introduction to Basic and Advanced Ridgeology, CRC Press, New York, 1999.

[8] S. Richmond, Do fingerprint ridges and characteristics within ridges change with pressure? Australian Federal Police Forensic Services, 2004. http://www.latent-prints.com/images/changes%20with%20pressure.pdf.

[9] A. Maceo, Qualitative assessment of skin deformation: a pilot study, J. Forensic Ident. 59 (4) (2009) 390–440.

[10] Federal Bureau of Investigation, Universal Latent Workstation (ULW), www.fbi-biospecs.org/Latent/LatentPrintServices.aspx.

[11] D. Maltoni, D. Maio, A. Jain, S. Prabhakar, Handbook of Fingerprint Recognition, 2nd ed., Springer, London, 2009.

[12] A. Jain, L. Hong, R. Bolle, On-line fingerprint verification, IEEE Trans. Pattern Anal. Mach. Intell. 19 (4) (1997) 302–313.

[13] C.I. Watson, D.P. Casasent, Correlation filters for recognition of live-scan fingerprints with elastic distortions, in: SPIE Optical Pattern Recognition XIV, vol. 5106, 2003, 1–12.

[14] A. Almansa, L. Cohen, Fingerprint image matching by minimization of a thin-plate energy using a two-step algorithm with auxiliary variables, Appl. Comput. Vis. (2000) 35–40.

[15] A. Bazen, S. Gerez, Fingerprint matching by thin-plate spline modeling of elastic deformations, Pattern Recognit. Lett. 36 (8) (2003) 1859–1867.

[16] F.L. Bookstein, Principal warps: thin plate splines and the decomposition of deformations, IEEE Trans. Pattern Anal. Mach. Intell. 11 (6) (1989) 567–585.

[17] A. Ross, S.C. Dass, A.K. Jain, Estimating fingerprint deformation, in: International Conference on Biometrics, vol. 3072, Hong Kong, (2004), pp. 249–255.

[18] A. Ross, S. Dass, A. Jain, A deformable model for fingerprint matching, Pattern Recognit. Lett. 38 (1) (2005) 95–103.

[19] O.S. Ushmaev, S.O. Novikov, Effectiveness of consideration of deformations in problems of fingerprint identification, Pattern Recognit. Image Anal. 18 (1) (2008) 151–155.

[20] X. Liang, T. Asano, H. Zhang, A combined radial basis function model for fingerprint distortion, vol. 4142, in: International Conference on Image Analysis and Recognition, 2006, 286–296.

[21] A. Senior, R. Bolle, Improved fingerprint matching by distortion removal, IEICE Transactions on Information and Systems E84-D (7) (2001) 825–831.

[22] D. Mital, E.K. Teoh, An automated matching technique for fingerprint identification, Ind. Electron. Control Instrum. 1 (1997) 142–147.

[23] National Institute of Standards and Technology, Special Database 27: Fingerprint Minutiae from Latent and Matching Tenprint Images, http://www.nist.gov/srd/nistsd27.cfm.

[24] National Institute of Standards and Technology, American National Standard for Information Systems: data format for the interchange of fingerprint, facial & other biometric information, ANSI/NIST-ITL 1-2011, 2011, http://fingerprint.nist.gov/standard.

[25] W. Chapman, et al., Latent Interoperability Transmission Specification. NIST Special Publication 1152, US Department of Commerce, National Institute of Standards and Technology, Washington, DC, 2013, http://nvlpubs.nist.gov/nist-pubs/SpecialPublications/NIST.SP. 1152.pdf.

[26] R.A. Hicklin, J. Buscaglia, Assessing the quality of friction ridge impressions, in: International Association for Identification Educational Conference, Louisville, KY, 2008.